On the Organization of Geostrophic Circulations Over Large Scale Topography by Eddy-Diffusion of PV

Malte Jansen

January 12, 2009

1 Introduction

The quasi-geostrophic (QG) potential vorticity (PV) for a homogeneous layer can be written as

$$q = \beta y + \zeta - f\frac{h'}{H} \tag{1}$$

where β is the planetary PV gradient ($\frac{\partial f}{\partial y}$), ζ is the relative vorticity, H is the mean depth of the layer and h' is a perturbation of the latter. For a layer bounded below by the bottom topography we can write:

$$q = \beta y + \zeta - f\frac{\eta}{H} + f\frac{h_b}{H}\,, \tag{2}$$

where η is the displacement of the interface bounding the layer at the top and h_b is the elevation of the bottom topography. A topographic feature can thus be viewed as an anomaly in the in the background PV field, similar to the β-effect.

Different theoretical concepts have been propasfosed arguing that quasi-geostrophic turbulence acts to "homogenize" the mean potential vorticity (PV) field which can be "disturbed" by topographic features. (See [7] for an older but still very useful review.) This homogenization would then lead to an anomaly in the relative PV field[1] over the topography which would be associated with a mean circulation.

Indeed observational evidence exists for this kind of circulations around topographic features. [8] first notized an almost barotropic 100Sv anticyclonic flow around the Zapiola Drift in the South Atlantic. A result later confirmed by various other observational studies.

Many previous theoretical and numerical studies focused on the adjustment of a turbulent flow in a closed domain in the abscence of forcing and with weak or no dissipation (e.g. [3] or [5]). [2], however, suggests that the strength of topographic circulations might be determined by a balance between the eddy flux of PV, and Ekman pumping due to bottom friction. Kinetic energy is in this case assumed to be provided by eddies from remote regions (such as the ACC for the Zapiola drift). The same approach is used in this study.

[1] relative PV is here used as the PV anomaly given by the displacement of the free interface and the relative vorticity

A simple qualitative explanation for the tendency of turbulent flows to homogenize PV can be given by assuming that stirring by geostrophic turbulence moves elements of fluid over the topography. Assuming that this happens on time-scales shorter than those of forcing and dissipation, these fluid elements will conserve their PV. If the fluid is stirred randomly so that each fluid parcel reaches each point of a domain with a similar average frequency, the time-mean PV has to be constant over that domain. If we further assume that the stirring "transports" inhomogeneities to smaller scales, until viscosity finally mixes the fluid irreversibly, the PV field will be homogenized.

Here we want to follow an approach used by [2] which is based on this idea of eddy-mixing. Treating PV as a conserved passive tracer we apply the commonly used approach of down-gradient eddy-diffusion. It should be noted that in doing this we ignore the fact that PV is not strictly a passive tracer since it's distribution determines the flow field. However, the results of eddy resolving numerical simulations, presented in this study, tend to support the use of this approximation.

An analytical derivation for the expected mean flow over topography in a two layer QG model assuming down-gradient diffusion of PV is shown in section 2. In section 3 the predictions of this theory are tested against eddy-resolving numerical simulations and section 4 presents some preliminary results from laboratory experiments. A concluding discussion of the results is given in section 5.

2 A Two Layer QG Model Assuming Down-Gradient Diffusion of PV

The two layer quasi-geostrophic PV equations on an f-plane with horizontal viscosity ν and linear bottom friction $F = -Ru$, can be written as

$$\left[\frac{\partial}{\partial t} + J(\psi_1,)\right] q_1 = \nu\nabla^4\psi_1 \tag{3}$$

$$\left[\frac{\partial}{\partial t} + J(\psi_2,)\right] q_2 = -R\nabla^2\psi_2 + \nu\nabla^4\psi_2 \tag{4}$$

where

$$q_1 = \nabla^2\psi + \frac{f}{H_1}\eta \tag{5}$$

$$q_2 = \nabla^2\psi + \frac{f}{H_2}(h_b - \eta)\,. \tag{6}$$

The shear between the two layers is given by the interface displacement η through the thermal wind relation

$$\psi_1 - \psi_2 = \frac{g'}{f}\eta\,. \tag{7}$$

Assuming that the eddy flux of PV can be described by down-gradient diffusion

$$\overline{u'q'} = -K\frac{\partial\bar{q}}{\partial x}, \tag{8}$$

the steady-state solution would be given by:

$$(K_1+\nu)\nabla^4\psi_1+\frac{K_1 f}{H_1}\nabla^2\eta=0 \tag{9}$$

$$(K_2+\nu)\nabla^4\psi_2+\frac{K_2 f}{H_2}\nabla^2(h_b-\eta)-R\nabla^2\psi_2=0\,, \tag{10}$$

where where the eddy diffusivity of PV, $K_{1/2}$ is allowed to be different in the two layers. If h_b, η and ψ_2 vanish somewhere outside the domain of interest , (9) gives:

$$\zeta_1\equiv\nabla^2\psi_1=-\frac{K_1}{K_1+\nu}\frac{f}{H_1}\eta\,. \tag{11}$$

Using (7), we find

$$\left(\frac{K_1+\nu}{K_1}L_{D_1}^2\nabla^2+1\right)\psi_1=\psi_2 \tag{12}$$

where $L_{D_1}^2=\frac{H_1 g'}{f^2}$. Hence we find a barotropic solution ($\psi_1\approx\psi_2$) if

$$\frac{L_{D_1}^2}{L^2}\ll\frac{K_1}{K_1+\nu}\,, \tag{13}$$

where L is the typical length-scale of the topographic mean flow which is assumed to be of the same scale as the topography itself. Note that the left hand side corresponds to the Burger number. With (13), we find from (11) that

$$\eta\approx-\frac{K_1+\nu}{K_1}\frac{H_1}{f}\nabla^2\psi_2 \tag{14}$$

and therefore

$$\frac{\eta}{H_1}\sim\frac{K_1+\nu}{K_1}Ro \tag{15}$$

where

$$Ro=\frac{U}{fL}\,. \tag{16}$$

We now find that (10) simplifies to

$$\psi_1=\psi_2=\frac{K_2 f}{RH_2}h\,, \tag{17}$$

if

$$\frac{L_{D_1}^2}{L^2}\ll\frac{K_1}{K_1+\nu}\,,\quad Ro\ll\frac{K_1}{K_1+\nu}\frac{h}{H_1}\quad\text{and}\quad Ro\ll\frac{K_2}{K_2+\nu}\frac{h}{H_2}\,. \tag{18}$$

Note that the first two conditions imply that $\eta\ll h$.

For sufficiently small Rossby and Burger numbers, we find a barotropic flow along isolines of constant depth controlled by an equilibrium between an eddy-diffusive flux of PV and bottom friction. This result is similar to the result obtained by [2] in the limit of a vanishing planetary vorticity gradient and wind-stress.

3 Numerical Simulations

The full set of equations (3) to (7) are integrated numerically. A list of parameters is given in table 3, they are chosen to resemble the laboratory experiments described later in this report. The topography used is given by a truncated cone centered in the middle of the domain. The length scale L_{top} given in table 3 denotes the length of the slope, the total diameter of the "bump" is $3L_{top}$. It should be noted that the topography is large compared to the deformation radius. Additionally to the truncated cone the topography is slightly parabolic (maximum amplitude about $0.1\,H_2$) over the whole domain to simulate the parabola arising due to the centrifugal force in the tank.

L_{domain}	L_{top}	L_D	H_1/H_2	h_b/H_2	f	R	ν
$150\,cm$	$17\,cm$	$1.5-2\,cm$	0.5	0.5	$3s^{-1}$	$0.01-0.08\,s^{-1}$	$0.01\,cm^2\,s^{-1}$

Table 1: Parameters used for the numerical simulations

The equations are intergrated using a pseudo-spectral[2] model with a grid spacing $\Delta \approx 0.6cm$. Considering that the typical eddy scale is a few times the deformation radius the model is eddy resolving. The model has periodic boundary conditions though a sponge layer is implemented along the boundaries which strongly damps PV perturbations and thus eliminates eddies that move into this boundary layer. The sponge layer was chosen to simulate an infinite domain in which eddies are allowed to move out of the area of interest. Turbulence was generated by four pairs of sources and sinks of PV located in the middle of the four sides of the square domain, right outside the sponge layer.

For the topography used in the simulation (17) gives a constant along-slope velocity

$$u_\phi = \frac{\partial \psi}{\partial r} = \frac{K_2 f}{R H_2}\frac{\partial h_b}{\partial r} = -\frac{K_2}{R}\frac{h_b f}{H_2 L_{top}} \equiv -\frac{K_2}{R}\beta\,, \tag{19}$$

where we defined β as the topographic PV gradient. Nondimensionalizing all variables using the deformation radius L_D as a length scale and $L_D^{-1}\beta^{-1}$ as a time scale gives

$$u_\phi^* = -\frac{K_2^*}{R^*}\,. \tag{20}$$

Two series of simulations are performed in which first the strength of the forcing was varied, and then the magnitude of bottom friction. Each simulation is run into a statistically steady state for at least 500 s. After this initialization period the PV fields of each layer are averaged over at least 1000 s. An overview of all simulations is given in table 2. Figure 1 shows an example of mean relative PV and streamfunction fields from the S04-3 simulation. We see the four PV sources which produce jets that get deflected to the right, which can be explained by the parabolic background PV field. Over the topography we observe anticyclonic circulations along the slope in both layers which is in qualitative agreement with (19). This is associated with negative relative PV in the lower layer and a positive relative PV in the upper layer, which is the PV disturbance expected from a positive displacement of

[2]Pseudo spectral here means that the product $\mathbf{u}q$ in the nonlinear advection term is calculated in grid-space and then transformed back into fourier space

the interface. The negative relative PV in the lower layer acts to reduce the topographic PV anomaly, though it does not completely compensate the latter which is as high as $\frac{fh_b}{H_2} \approx 1.7$. Moreover we can find that a strong PV anomaly is only found on the lower part of the slope with a relatively sharp transition to a smaller PV anomaly further inside. This indicates a "PV staircase" as suggested by [7] due to a limitation of the coss-slope eddy mixing length to the Rhines-scale ($L_R = \sqrt{u/\beta}$) which is of the same order as the deformation radius here.

Name	S01	S02	S04-1	S04-2	S04-3	S08	S16	S32	R1	R2	R4	R8
Source $[s^{-2}]$	0.1	0.2	0.4	0.4	0.4	0.8	1.6	3.2	0.4	0.4	0.4	0.4
R $[10^{-2}s^{-1}]$	2	2	2	2	2	2	2	2	1	2	4	8

Table 2: List of performed numerical simulations. The second line gives the peak absolute value of the vorticity sources and sinks and the last line gives the bottom drag. The deformation radius L_D was 2 cm for simulations S01-S32 and 1.5 cm for simulations R1-R8. All other parameters are as given in table 1.

For a more quantitative analysis the mean along slope velocity was calculated for each performed simulation. Figure 2 shows the non-dimensional mean along-slope velocity from simulations S01 to S32 against the non-dimensional mean lower layer Eddy Kinetic Energy (EKE) averaged over the whole domain of integration and against the EKE averaged only over the topography. A first observation is that the along slope velocity increases with EKE. Since we expect the eddy diffusivity to rise with EKE, this is in qualitative agreement with the theoretical prediction (20). However, while the flow is anticyclonic in both layers, the magnitude is quite different in some simulations, especially for those with low EKE where we find a stronger anticyclone in the upper layer then in the lower layer. As the strength of the sources is inreased and the EKE becomes higher, the flow becomes more barotropic with the anticyclone in the lower layer being somewhat stronger than in the upper layer for high EKE. Focussing on the lower layer velocities and the EKE over the topography (which we assume is a better predictor for the eddy dissusivity in this area) we find that the along-slope velocity approximately grows as $EKE^{3/4}$.

The left panel in figure 3 shows the along-slope velocity versus the inverse of the bottom friction for experiments R1 to R8. The linear increase of u^*_ϕ with $1/R^*$ appears to be in good agreement with (20), assuming that the eddy-diffussivity does not change between the experiments. This, however, can not necessarily be expected.

To allow for a better test of prediction (20), two different methods were used to estimate the eddy-diffussivity K_2 and how it relates to EKE.

The eddy-flux of PV can generally be decomposed into a down-gradient flux and a bolus flux along iso-lines of PV as follows:

$$\overline{\mathbf{u}'q'} = \frac{\overline{\mathbf{u}'q'} \cdot \nabla\bar{q}}{|\nabla\bar{q}|^2}\nabla\bar{q} - \frac{\overline{\mathbf{u}'q'} \times \nabla\bar{q}}{|\nabla\bar{q}|^2} \times \nabla\bar{q} \tag{21}$$

$$\equiv \quad -K\nabla\bar{q} \qquad + \qquad \psi_B \times \nabla\bar{q}\,. \tag{22}$$

Using this formulation we can calculate the actual PV-diffussivity K and bolus stream-function ψ_B from time averages of the numerical integration. While ψ_B is rather indistin-

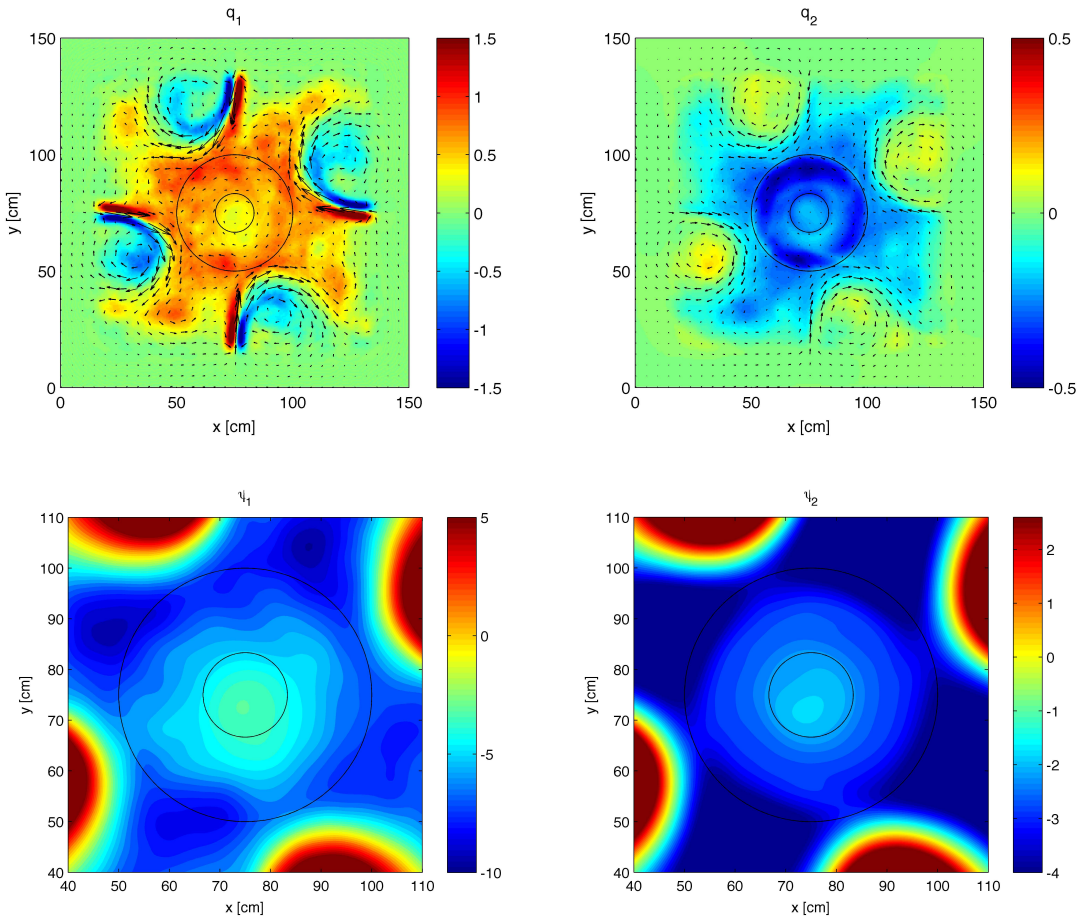

Figure 1: Mean relative PV in s^{-1} and velocity vectors (top) and streamfunction in $cm^2 s^{-1}$ (bottom) for simulation S04-3. The upper layer is shown on the left and the lower layer is shown on the right. The black circles indicate the topography, with the outer circle representing the outer edge of the cone and the inner circle representing the truncated top.

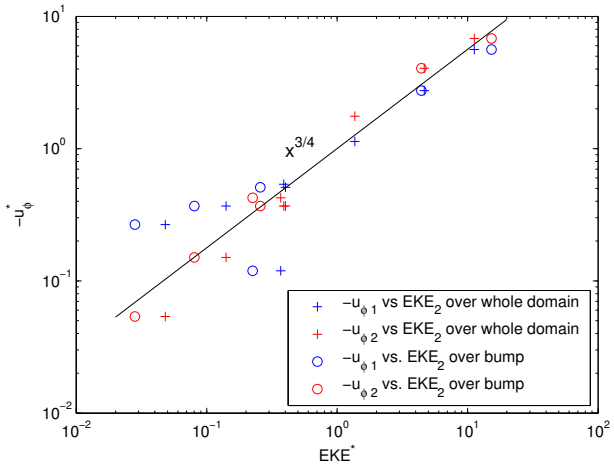

Figure 2: Non-dimensional mean along-slope velocity u_ϕ in the upper (blue) and lower layer (red) for simulations S01 to S32 vs. the (non-dimensional) mean EKE averaged over the whole domain of integration (crosses) and against the EKE averaged over the topography (circles).

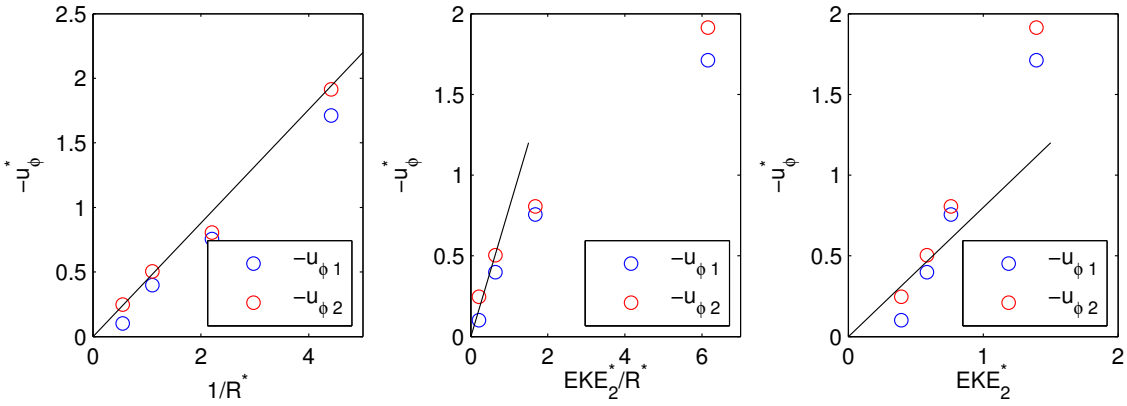

Figure 3: **Left:** Non-dimensional mean along-slope velocity u_ϕ in the upper (blue) and lower layer (red) for simulations R1 to R8 against the inverse of the non-dimesional friction parameter $(1/R^*)$. **Center:** As left, but u_ϕ against EKE^*/R^*, where EKE^* denotes EKE averaged over the topography. **Right**: As left but u_ϕ against EKE^*

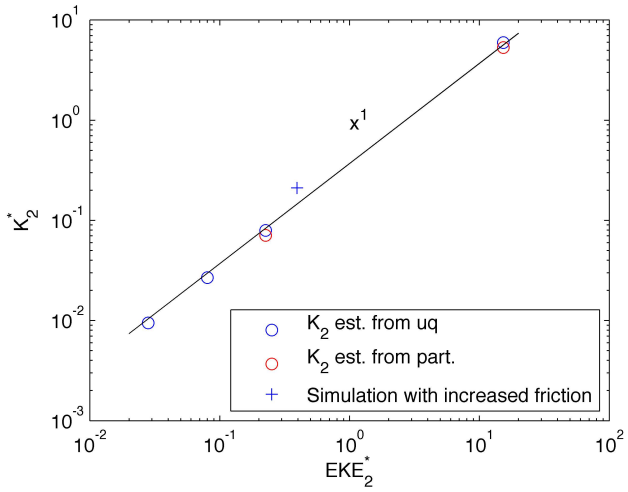

Figure 4: Lower level eddy-diffussivity K_2^* over the topographic slope, estimated from (22) (blue) and from (23) (red) against EKE^* over the topography. The circles show data from experiments S01, S02, S04-3 and S32. The cross shows an estimate from R8.

guishable from noise in both layers, for the data available, the lower layer diffussivity K_2 is found to be coherently negative over the slope of the topography, which retrospectively justifies the down-gradient diffusion parameterization used in the theory presented above. An averaged eddy-diffussivity over the slope is calculated this way.

This direct calculation of PV diffusion is compared to the diffusion of a conserved tracer obtained from particle release simulations. For two experiments (S04-3 and S32) 1000 particles were placed in a circle along the topographic slope. The diffussivity can be estimated using

$$4K = \frac{\partial}{\partial t}\left\langle \frac{1}{N}\sum_i r_i^2 \right\rangle , \tag{23}$$

where N is the total number of particles and r_i is the distance of each particle from the center. Since we are interested in estimating the diffussivity above the slope, we evaluate (23) only until the particles leave the slope-area. To increase the accuracy of the estimate, the tracer release was repeated 5 and 8 times in succession for the S04-3 simulation and the S32 simulation, respectively. A possible error in this estimate up to a factor of two however, should still be considered.

Figure 4 shows the eddy-diffusivity over the slope in the lower layer, estimated in this two ways versus the lower layer EKE over the topography. Note, that for the two experiments for which both methods were applied, the eddy diffussions of PV calculated directly from (22) agree well with the diffussivity estimates from the particle release simulations. We further find that the eddy diffussivity scales convincingly like

$$K^* \sim EKE^* , \tag{24}$$

though simulation R8 for which Ekman friction was increased by a factor of four deviates somewhat from this scaling. This result might come rather surprising considering that for

a fully turbulent flow we expect a scaling like

$$K \sim U_{eddy} L_{eddy} \tag{25}$$

with typical eddy velocities and scales U_{eddy} and L_{eddy}, respectively. Assuming that L_{eddy} scales like the deformation radius this becomes, in non-dimensional parameters

$$K^* \sim U^*_{eddy} \sim \sqrt{EKE^*}\,. \tag{26}$$

This is not observed, probably because flow over the slope is not fully turbulent. Comparing the nonlinear advection term of the QG PV equation with the advection of topographic PV (the topographic β-term) we find a "nonlinearity -parameter"[3]

$$N \equiv \frac{J(\psi, \nabla^2\psi)}{\frac{1}{r}\frac{\partial\psi}{\partial\phi}\beta} \sim \frac{L_R^2}{L_D^2} = U^*_{eddy}\,, \tag{27}$$

where $L_R = \sqrt{\frac{U_{eddy}}{\beta}}$ is the topographic Rhines scale. N ranges around 0.2 to 5 in the simulations shown here, indicating that the assumption of fully developed turbulence is rather inadequate. Considering that (undamped) linear motion does not contribute to mixing we can argue that the eddy-diffusion in this weakly nonlinear case is given by the traditional scaling for turbulent motion (25) times this nonlinearity-parameter which would give

$$K^* \sim U^*_{eddy} N \sim EKE^*\,. \tag{28}$$

However, to some extend any power of N and thus any power of U^* could be justified this way. Since the eddy scale is generally larger than the deformation radius, which makes the effective nonlinearity even smaller than the above estimate, we could argue that the motion over the slope is in a regime of linear damped waves. In this case the "eddy diffussivity" would be given by

$$K = \int u(t)u(t+\tau)d\tau \sim \frac{U^2 R}{R^2+\omega^2} \approx \frac{U^2 R}{\omega^2} \tag{29}$$

where ω is the frequency, U is the velocity perturbation associated with the wave motion and R is the coefficient of bottom friction (see above). The approximation on the right-hand side holds for weakly damped waves. Assuming that the wave length scales like the deformation radius and the corresponding frequency is given by the Rossby-wave dispersion relation we find, in non-dimensional parameters

$$K^* \sim \frac{U^{*2} R^*}{R^{*2}+1} \approx U^{*2} R^* = EKE^* R^*\,. \tag{30}$$

This limit can explain the observed linear scaling of K^* with EKE^*. However, the calculated eddy diffussivity for simulation R8 agrees somewhat less with (30) than with (28). Plotting K^* vs. EKE^*R^* shows that the diffussivity of R8 lies significantly below the line $K^* \sim EKE^*R^*$ (not shown).

The center and right panels of figure 3 show the along slope velocity versus EKE^*/R^* which would be expected to be linear from (20) and assuming the scaling law (28), and versus

[3]The inverse of this parameter is sometimes referred to as"steepness".

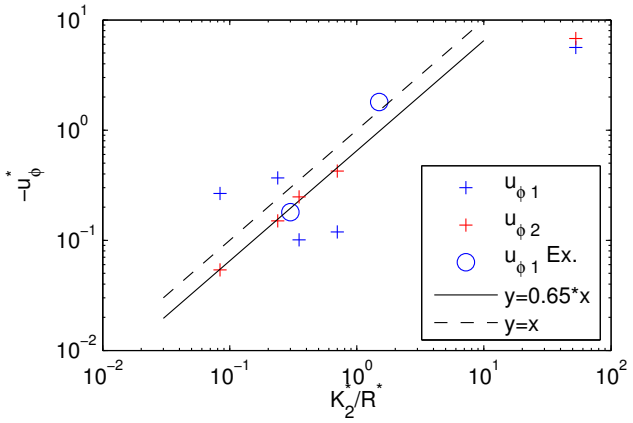

Figure 5: Non-dimensional along-slope velocity u^*_ϕ in the upper (blue) and lower layer (red) versus K^*_2/R^* for all simulations for which K_2 was explicitly calculated (S01, S02, S04-3, S32 and R8). The circles show two experimental results (see text). The solid straight line denotes $-u^*_\phi = 0.65 \cdot K^*_2/R$ and the dashed line shows $-u^*_\phi = K^*_2/R$ which is the theoretical result (20).

$EKE*$ which would be expected to be linear assuming scaling law (30), for simulations R1 to R8. Both relations appear rather non-linear, suggesting that both scaling laws might be inadequate to describe the scaling of the eddy diffusivity under variation of bottom friction, found here.

The most direct test of the theoretical prediction (20) is given by figure 5 which shows the along-slope velocity in both layers versus K^*_2/R^* for all simulations for which K_2 was explicitly calculated. As mentioned before, we note the lack of barotropization especially for low-EKE simulations, which was expected from the theory. For the lower layer, however, we find good agreement with the theory as long as the EKE does not become too large. For high EKE (i.e. high eddy diffussivity) the results indicate a deviation towards lower along-slope velocities than expected from (20).

4 Experimental Results

In a second step the theory shall be verified by laboratory experiments. Experiments were conducted in a rotating tank using a two layer fluid. The density difference was obtained using water with slightly different salinity. The reduced gravity for the experiment shown here is $g' = 4cms^{-2}$. The rotation rate gives $f = 4s^{-1}$, which results in a deformation radius $L_D \approx 2cm$. A truncated cone is placed in the center of the tank as in the numerical simulations. A sketch of the experiment is shown in figure 6. Eddies are generated by four pairs of sources and sinks in the upper layer equally spaced around the tank. The method is described in detail in [4].

Since the expected along-slope velocities are on the order of $1mms^{-1}$ or less the experiment, and especially the filling up of the upper layer, has to be done very carefully. A series of similar experiment has previously been performed by [6], but the results are not used

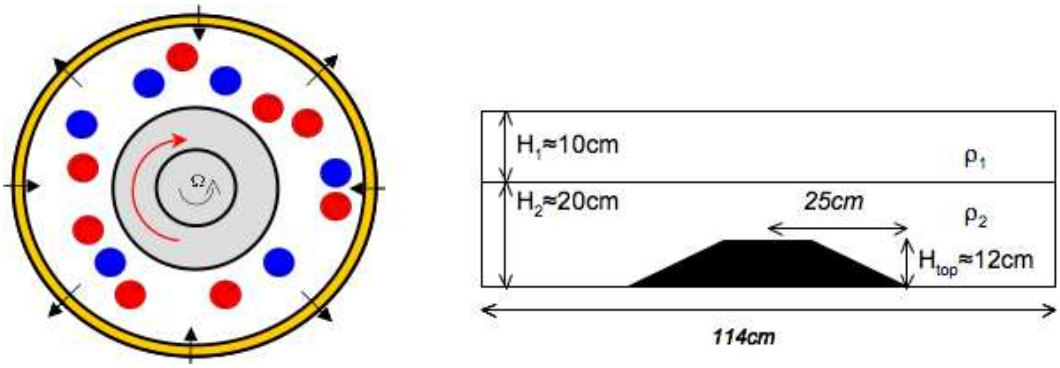

Figure 6: Sketch of the experimental setup. Left: Topview. The arrows on the tank wall indicate sources and sinks in the upper layer to generate pairs of cyclonic and anticyclonic eddies, indicated in red and blue. Right: Side view. The figure on the left is taken from [1].

here, mainly because a review of the lab-recordings suggested that the filling-up procedure in these experiments might have had a significant influence on the observed circulation, which can hardly be filtered out in hindsight. Due to similar and other problems during this study, only the results of one experiment will be discussed here. However, the flow rate of the sources and sinks was increased by a factor of 1.7 during this experiment, so that two different values of the flow rate are presented. The first part of the experiment, with a flow rate of 540 cc/min per jet, will be referred to as Ex3, while the second part, with a flow rate of 920 cc/min per jet, will be refferred to as Ex3.5, in the following. Since the diffusion of the interface between the two layers is significantly enhanced due to the eddy activity, it is likely that a sharp interface did not exist any more during Ex3.5, which therefore has to be handled with care.

Figure 7 shows a series of snapshots from Ex3. Neutrally buoyant dye, released from outlets on the bottom of the cone, indicates an anticyclonic circulation around the cone in the lower layer, with an average velocity of the order of $-u_{\phi 2} \approx 0.3mm/s$. The flow in the upper layer can be evaluated more quantitatively by tracking of surface particles which can also be seen in figure 7. Two 30-minute time averages of surface velocity and vorticity from Ex3 are shown in figure 8. The most striking feature that is observed is a strong cyclone above the flat center of the truncated cone. It should be noted that the frame-rate used for the particle tracking was slower for the figure shown on the left, which causes an inadequate resolution of the fast cyclone observed over the top of the cone. The cyclone remained above the flat center of the cone during the whole time of the experiment. Dye releases in the lower layer indicate an associated cyclonic motion in the lower layer, though probably weaker. A similar feature is not predicted by theory and was never observed in the numerical simulations. It should be noted that the Rossby-number for this cyclone is O(1), which might explain it's absence in the numerical QG model. A physical explanation for this observation, however, is still outstanding. Over the slope itself we observe an anticyclonic circulation as predicted by the theory. The averaged along-slope velocity in the upper layer is $-u_{\phi 1} \approx 0.9mm/s$ and thus probably stronger than in the lower layer, similar to the results found in the numerical simulation for rather small EKE. We further

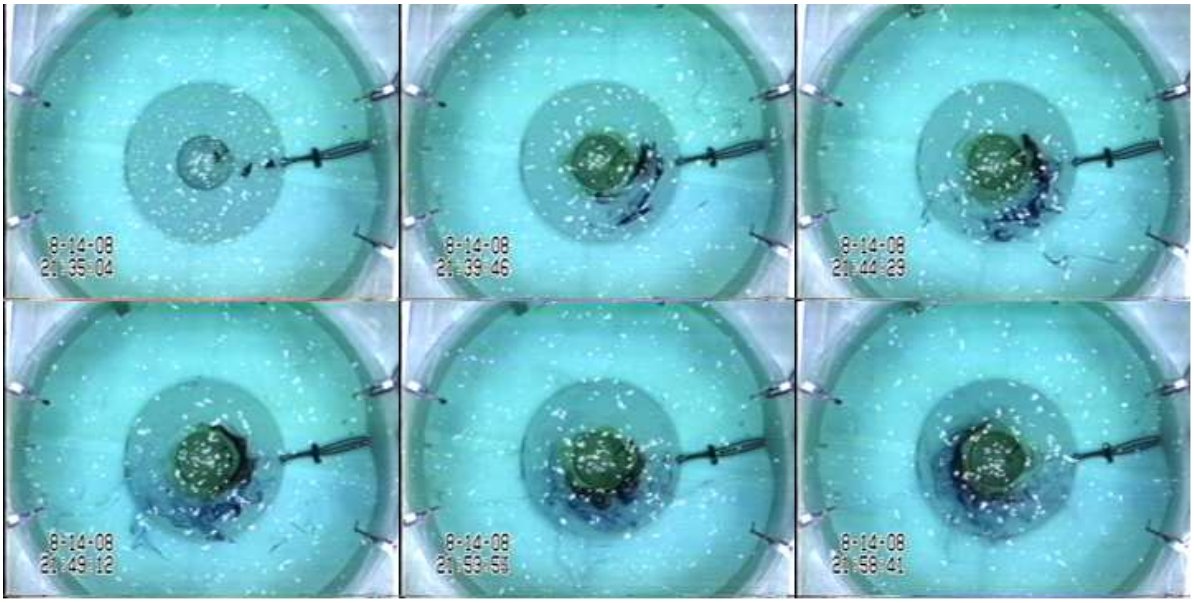

Figure 7: Series of snapshots from Ex3. Time elapses from the top left to the bottom right with the time difference between each snap-shot being about 4min 45s. One can see the dye in the lower layer traveling anticyclonicly along the topographic slope.

observe a band-like vorticity structure. This was previously mentioned in the discussion of the numerical results and probably indicates a PV-staircase as discussed by [7].

Figure 9 shows a ten minute average[4] of surface velocity and vorticity from Ex3.5, i.e. with increased flow rate. Since the kinetic energy of the fluid injected by the sources scales with the square of the flow-rate, and the amount of fluid with that kinetic energy scales linearly with the flow rate, we expect the kinetic energy injected per time to scale like the cube of the flow rate. Assuming linear dissipation, we thus expect the EKE in the tank to rise approximately like the cube of the flow rate. An increase of the flow rate by a factor of 1.7 should therefore cause an increase of the EKE by a factor of $1.7^3 \approx 5$. Using the scaling (28) or (30), the theoretical result (20) would therefore suggest an increase of the along-slope velocity by a factor of 5. The experiments show an increase of the mean along-slope velocity by about a factor of ten The estimated upper layer mean velocity over the slope for Ex3.5 is $-u_{\phi 1} \approx 9\, mm/s$.

The results of experiments Ex3 and Ex3.5 are added to figure 5. Since no good estimate for the eddy diffussivity exists for the experiments exists, for Ex3 K_2^* is fitted to match with the numerical results. For Ex3.5 K_2^* was then chosen to be five times this value, following the argumentation above. Due to the "tuning" of the diffussivity of Ex3, the comparison to the numerical result has some limitations. However, figure 5 indicates that the experiments are in a regime well covered by the numerical study. Also the slope between the two experimental data points, which is not affected by this tuning, shows general agreement with the numerical results. Note, that the used EKE estimate provides an estimate for EKE

[4]Since the faster flow allows for a reasonable average in a shorter time and the strong eddy activity in Ex3.5 caused the interface to be destroyed more rapidly, a shorter time average is used in Ex3.5 then in Ex3.

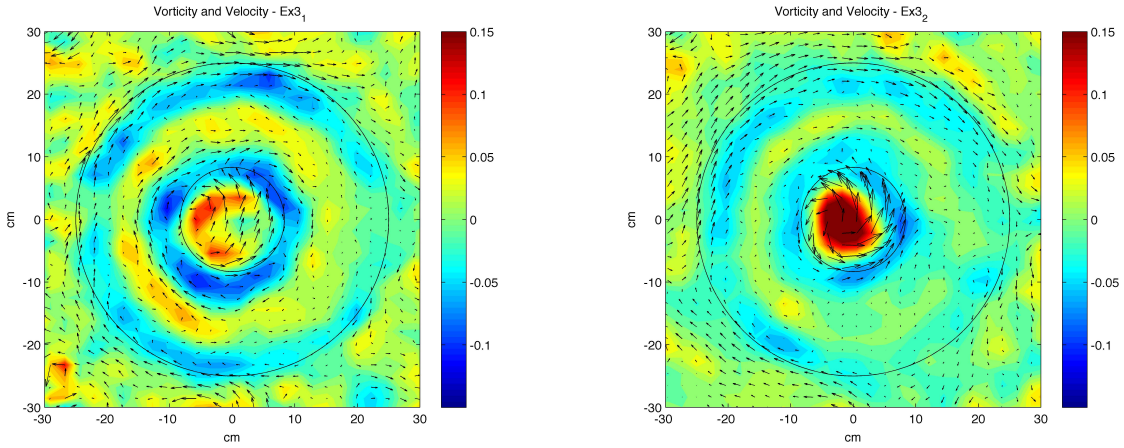

Figure 8: Two different eulerian mean velocity fields and the resulting vorticity, each averaged over about 30 minutes of EX3. The average field shown on the left was taken about one hour earlier than the field on the right. Velocity vectors are stretched by a factor of 10. The solid lines indicate the truncated cone.

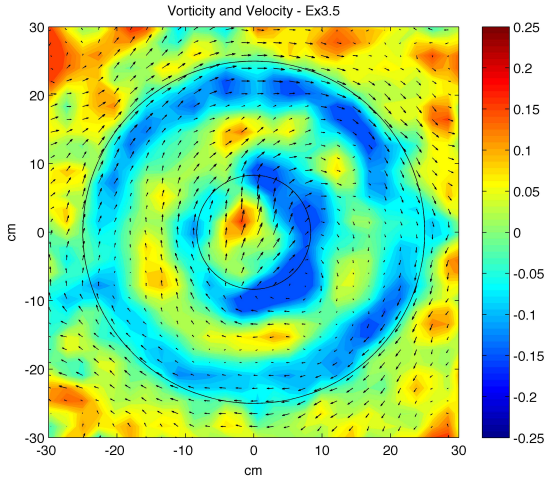

Figure 9: Eulerian mean velocity fields and the resulting vorticity each averaged over about 10 minutes of EX3.5. Velocity vectors are stretched by a factor of 2

averaged over the whole domain and not over the topography itself. The numerical models showed that the latter might grow faster with increased forcing, since the topographic PV gradient prevents weak eddies to propagate over the topography. Note also, that, due to the better measurability, the experimental results show upper layer velocities. As in the numerical simulations, however, the flow was not strictly barotropic.

5 Summary and Discussion

Assuming down-gradient eddy-diffusion of potential vorticity it was shown that in a two layer QG model for small Rossby numbers an approximately barotropic mean along-slope circulation is expected to arise over an isolated topographic feature which is anticyclonic for a mount and cyclonic for a depression. The strength of the circulation is controlled by an equilibrium between the eddy flux of PV and bottom friction. This prediction was tested using numerical simulations performed with an eddy resolving two-layer QG model and laboratory experiments.

The numerical simulations reproduce an anticyclonic along-slope circulation in both layers over a mount. However, especially for low EKE, the magnitude of the circulation is significantly different in the two layers, which disagrees with the theoretical prediction of a barotropic flow. Part of this inconsistency might be explained by a direct influence of the forcing. The latter consists of four pairs of PV sources and sinks in the upper layer which generate jets penetrating towards the center of the tank. The jets get unstable and generate eddies. These jets, however, could have a significant direct influence on the circulation in the upper layer, especially in the less turbulent simulations with low EKE.

The eddy diffussivity was estimated for a series of experiments. The results suggest a down-gradient diffusion of PV over the topography of similar magnitude as the eddy diffussivity of a passive tracer. It was further found that in the performed simulations the eddy-diffussivity over the slope scales linearly with the EKE, which suggests a linear or weakly nonlinear motion over the slope. However, no scaling law was found which consistently describes the dependence of the observed eddy diffussivity on bottom friction. It is likely that the experiments are covering a transition between a regime of fully linear damped waves and weakly nonlinear motion, for which case the dependence on bottom friction is expected to change over the range of performed experiments.

In the simulations for which the eddy diffusivity is calculated explicitely, the lower layer velocity agrees well with the theory in the range of lower and medium eddy diffussivity, but the along-slope velocity is smaller than the theoretical prediction for high eddy diffussivity.

It seems desirable to test whether the differences between the eddy resolving numerical simulation and the theoretical results, are mainly a shortcoming of the down-gradient diffusion parameterization or due to additional approximations made for the analytical solution. Preliminary results, not shown above, solving the full two layer QG model numerical without forcing but using a down-gradient diffusion parameterization, indicate that the differences are mostly a shortcoming of the down-gradient diffusion parameterization (including the lack of a representation of the direct effect of the forcing) and not dominantly due to inappropriate additional approximations made to obtain a simple analytical solution. Adding an additional eddy-viscosity seems to improve the results, though no convincing physical justification for this is known to the author.

Laboratory experiments using a two-layer fluid in a rotating tank do also reveal an anticyclonic flow along the topographic slope, which is in qualitative and to a lesser extend quantitative agreement with the theory. However, additionally a strong cyclone was observed over the flat center of the topography. An explanation for this observation is so far outstanding. More, carefully performed, experiments would be necessary to test the theoretical predictions in a more quantitative way.

6 Acknowledgments

I would like to thank Claudia Cenedese for her support during the whole project. Thanks to Bill Dewar for sparking my interest in this problem and to Raffaele Ferrari and John Whitehead for fruitfull discussions. Special thanks to my fellow fellows for many great scientific discussions and a good time.

References

[1] C. Cenedese and W. K. Dewar, *Collaborative research: The zapiola blender*. Project Proposal submitted to NSF.

[2] W. K. Dewar, *Topography and barotropic transport control by bottom friction*, J. Mar. Res., 56 (1998), pp. 295–328.

[3] G. Holloway, *Systematic forcing of large-scale geophysical flows by eddy-topography interaction*, J. Fluid Mech., 184 (1987), pp. 463–476.

[4] P. F. Linden, B. M. Boubnov, and S. B. Dalziel, *Source–sink turbulence in a rotating stratified fluid.*, J. Fluid Mech., 298 (1995), pp. 81–112.

[5] D. P. Marshall, S. T. Adcock, and C. E. Tansley, *Geostrophic eddies, abyssal recirculations, and zonal jets*, 2001. Conference paper.

[6] R. B. D. Mesquita, *Experimental study of bottom controlled flow over isolated topography.*, 2006. "Laurea" Thesis, University of Rome "La Sapienza", Rome, Italy.

[7] P. B. Rhines, *Geostrophic turbulence*, 11 (1979), pp. 401–441.

[8] P. Saunders and B. King, *Bottom currents derived from a shipborne ADCP on WOCE cruise A11 in the South Atlantic.*, J. Phys. Oceanogr., 25 (1995), pp. 329–347.